1

Quantification Improvements of ^{1}H MRS Signals

Maria I. Osorio-Garcia[1], Anca R. Croitor Sava[1], Diana M. Sima[1], Flemming U. Nielsen[2], Uwe Himmelreich[2] and Sabine Van Huffel[1]
[1]*Dept. Electrical Engineering, ESAT-SCD, Katholieke Universiteit Leuven*
IBBT - K.U. Leuven Future Health Department
[2]*Biomedical Nuclear Magnetic Resonance Unit, Katholieke Universiteit Leuven*
Belgium

1. Introduction

In vivo ^{1}H Magnetic Resonance Spectroscopy (MRS) and Magnetic Resonance Spectroscopic Imaging (MRSI) signals contain relevant metabolic information commonly used as biomarkers of diseases that can provide complementary information for the diagnosis. These signals are measured in the time domain, however, their representation in the frequency domain provides a better visualization of the metabolites in the form of resonances (peaks). In ^{1}H MRS(I), not only metabolites but also water and macromolecule/lipid resonances can be observed. In practice, the concentrations of metabolites and the presence of macromolecule/lipids contain the relevant information for diagnosis purposes.

The technique used to determine metabolic contributions is called quantification and different methods have been proposed in the time or the frequency domain. In these methods, the metabolite concentrations are estimated, *e.g.*, using a linear combination of individual peaks or a basis set of known metabolite profiles to fit the MR signal (Poullet et al., 2007; Provencher, 1993; 2001; Ratiney et al., 2004; Slotboom et al., 1998). No matter which quantification method is used, the quality of MRS signals is important for obtaining accurate estimates of the metabolite concentrations.

Although *in vivo* MRS(I) acquisitions provide non-invasively metabolic information, different limitations related to the specifications of the acquisition protocol, the localization of the voxels of interest and the homogeneity of the magnetic field in the selected region make the accurate quantification of these signals still a challenge. Therefore, advanced and efficient measurements have been developed to decrease the scanning time and to increase the spectral resolution. Nevertheless, it is essential to perform a series of preprocessing steps to improve spectral quality of MRS signals before performing quantification. Successful combinations between advanced acquisition techniques and appropriate signal processing increase the potential of integrating MR techniques in the clinical diagnosis routines (Chu et al., 2003; Devos et al., 2004; Huang et al., 2001; Ruiz-Pena et al., 2004; Vermathen et al., 2003).

In the next sections, we introduce the MRS(I) signals together with some of the most common preprocessing and quantification methods. In particular, we focus on recent methods and approaches to improve the quantification of *in vivo* MRS(I) signals, performed with

the quantification method AQSES (Poullet et al., 2007): *a*) filtering of residual water, *b*) lineshape estimation, *c*) baseline estimation and *d*) inclusion of spatial constraints in MRSI quantification.

2. Description of ^{1}H MRS(I) signals and preprocessing methods

2.1 ^{1}H MRS(I) signals

These signals are measured in the time domain and have ideally a decaying shape, also called FID, which can be represented as a sum of complex-damped exponentials. They can be measured from a specific anatomical region (single voxel MRS), or from an entire organ overlaid by a grid of multiple voxels (MRSI). In order to observe the contribution of individual metabolites, MRS(I) signals are transformed to the frequency domain using the Fast Fourier Transform (FFT), producing a spectrum where the metabolite resonances can be visualized. Typically, a water suppression technique is applied as part of the acquisition protocol in order to enhance the visualization of the metabolites of interest. Additionally, an unsuppressed water signal is always measured, which is commonly used as a reference for phase, eddy currents and lineshape corrections. Depending on the acquisition protocol, single voxel signals have commonly a better signal-to-noise (SNR) ratio and thinner linewidths than multi-voxel signals, however, the advantage of multi-voxel signals is the possibility to study complete anatomical organs using one acquisition. See Fig. 1 for an example of a single and multi-voxel acquisition.

2.2 Preprocessing ^{1}H MRS(I) signals

Preprocessing of MRS signals aims at the improvement of signal quality in order to accurately extract relevant information about the metabolites via the technique called quantification. Some essential preprocessing procedures in ^{1}H MRS(I) are:

- **Time circular shift**. The digital filter and decimation in the Bruker scanners distort the beginning of the FIDs, as a consequence, the MR spectrum is filled with wiggles and the metabolite resonances are hard to identify. These first data points are initially zero and then increase, until the actual FID starts (Cobas & Sardina, 2003). A solution to this distortion is a time circular shift. This step is performed in the time domain and consists of removing data points from the beginning and adding them to the end of the signal.
- **Frequency alignment**. Due to variations in the physiological and experimental conditions (*e.g.*, temperature and pH), MR resonances experiment a frequency shift. Specially in multivariate analysis, this peak misalignment needs to be corrected. Thus, the FIDs are first transformed to the frequency domain and the spectra are shifted such that some recognizable peaks reach the desired frequency locations (Veselkov et al., 2009). In ^{1}H MRS, the resonance frequency of known metabolites can be used for shifting the full spectra. For instance, the peak of N-Acetyl-Aspartate (NAA) is known to be located at 2.01 ppm. Moreover, the displacement of individual spectral peaks from one metabolite can be corrected using advanced frequency alignment techniques, such as, quantum mechanics approaches and advanced warping algorithms (Giskeødegård et al., 2010; Lazariev et al., 2011).
- **Phase correction**. Ideally, MRS spectra should have zero-phase (*i.e.*, all peaks are pointing upwards), however, differences between the reference phase and the receiver detector

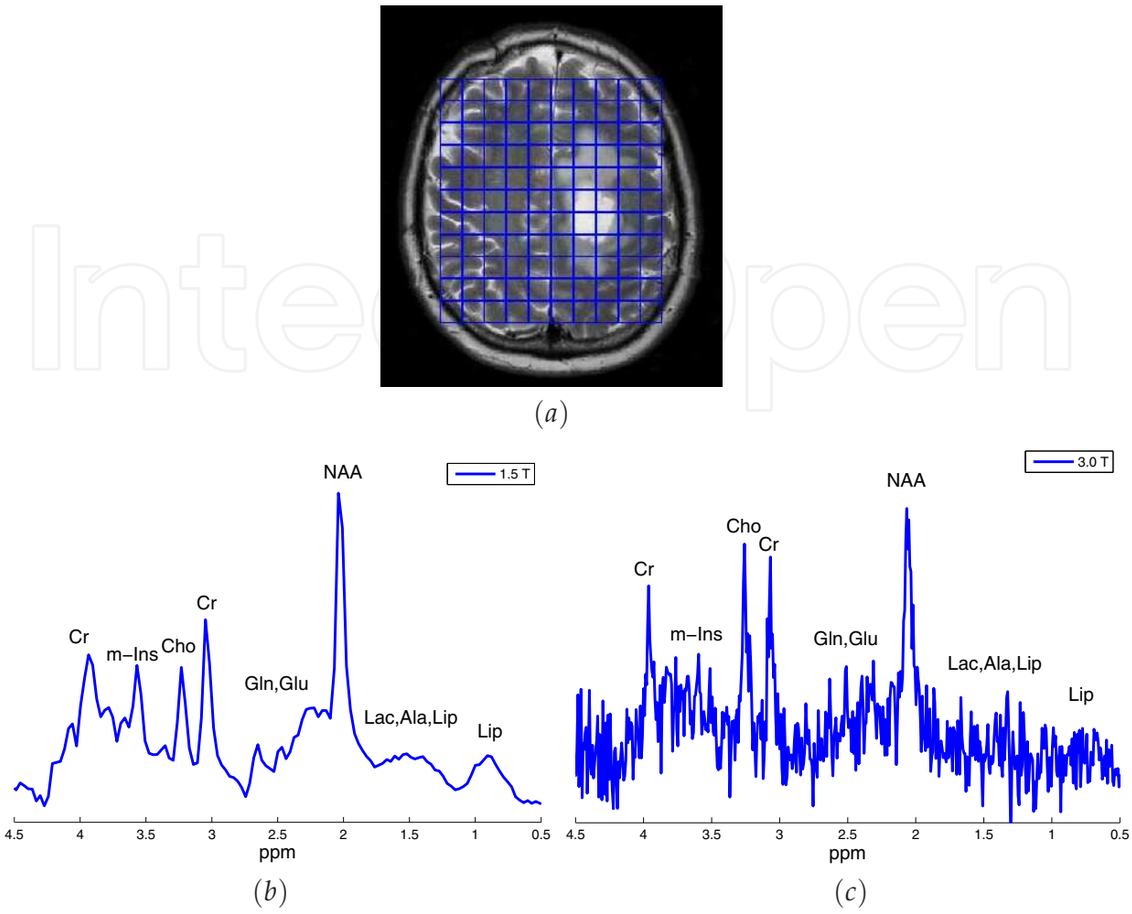

Fig. 1. (a) T2-weighted MRI of a brain tumor patient overlaid with a grid of voxels corresponding to an MRSI measurement. (b) Real part of the spectrum of a single voxel *in vivo* MRS signal acquired with a 1.5 T Philips NT Gyroscan (Philips Medical Systems, Best, The Netherlands) with acquisition parameters: PRESS sequence, repetition time (TR)=6 s, echo time (TE)=23 ms, bandwidth (SW)=1 KHz, number of points (NDP)=512 points and 64 averages. (c) Real part of the spectrum of a signal from a selected multi-voxel (MRS(I)) measurement acquired with a 3.0 T Philips Achieva (Philips Medical Systems, Best, The Netherlands) with acquisition parameters: PRESS sequence, TR=2 s, TE=35 ms, SW=2 KHz and NDP=2048 points and 1 average. These measurements were done at the University Hospital of the Katholieke Universiteit Leuven, Belgium.

phase, the time delay between the excitation and detection, the flip-angle variation across the spectrum, and the phase shifts from the filter employed to reduce noise outside the spectral bandwidth, produce different phase distortions (Chen et al., 2002). As a solution, phase correction approaches have been successfully used to improve the visualization of MR spectra. In practice, the phase correction consists of two components, one frequency-dependent (first order phase) and one frequency-independent (zero order phase). In particular, the zero-order phase correction consists of the multiplication of the complex spectrum by a complex phase factor equal to the initial phase of the FID (Jiru, 2008). On the other hand, adjusting the first order phase corresponds to the modification of the begin time of the MR signal (Chen et al., 2002). Although some quantification

methods (Poullet et al., 2007; Provencher, 2001; Ratiney et al., 2005) are able to take into consideration phase distortions and provide accurate metabolite estimates even if the spectra are not zero-phased, other quantification methods, such as peak integration, require zero-phased spectra in order to obtain reliable metabolite estimates.

- **Eddy current corrections**. These currents are induced by the rapid switching of the magnetic field gradient in the magnet coils and surrounding metal structures (de Graaf, 1998). Because these currents are caused by the scanner and can not always be avoided, a spectral correction is necessary. Klose (Klose, 1990) has developed a method to correct eddy currents, called ECC, by point-wise dividing the water suppressed signal by the phase term of the water unsuppressed signal measured at the same location.
- **Lineshape correction/estimation**. The lineshape of MR signals is determined by the decay function (damping) of the time domain signal and refers to the shape of the peaks in the frequency domain. Ideally, it is represented by a Lorentzian, Gaussian or Voigt function, corresponding in the time domain to an exponentially decaying sinusoid. However, when magnetic field perturbations and field inhomogeneities are present, these lineshapes are disturbed (in symmetry and linewidth) and as a consequence, the ideal model used in the quantification method is unable to yield accurate metabolite estimates. Therefore, different hardware and mathematical approaches have been developed to cope with this problem. For instance, shimming techniques (*i.e.*, coils adjustment) are applied during the MR acquisition in order to correct field inhomogeneities and thus improve spectral quality (Blamire et al., 1996; Gruetter, 1993; Juchem et al., 2010). Moreover, local magnetic field susceptibility problems caused by measurements near an air cavity such as sinuses, may not always be corrected with shimming techniques making lineshape distortions unavoidable. Notwithstanding, some preprocessing methods have been successfully used based on the deconvolution of the spectra using either the unsuppressed water signal or a reference peak from the experimental signal (Bartha et al., 2000; de Graaf et al., 1990; Metz et al., 2000). Alternatively, other lineshape estimation methods based on self-deconvolution have been proposed in cases when a reference signal is not available (Maudsley, 1995; Popa et al., 2011; Sima et al., 2009).
- **Baseline correction/estimation**. ^{1}H MRS signals measured at short TE contain not only information from metabolites but also from lipids and macromolecules which may affect the baseline of the spectra. This baseline influences the quantification causing the mis-fitting of individual peaks or metabolite profiles. Therefore, different correction algorithms have been proposed to estimate and remove the baseline contribution from the spectrum (Chang et al., 2007; Cobas et al., 2006; Xi & Rocke, 2008). Alternatively, other methods have been proposed to estimate the baseline using special acquisition protocols or characterizing each macromolecule/lipid component to finally consider them in the quantification procedure (Behar & Ogino, 1993; Hofmann et al., 2001; Knight-Scott, 1999).
- **Filtering of residual water**. ^{1}H MRS signals contain a water peak thousands of units larger than those of metabolites. Therefore, in order to visualize metabolites, this water peak needs to be suppressed. Although the water resonance is partially suppressed during acquisition, the residual water requires a reliable filter for further elimination without affecting the metabolite resonances. Moreover, especially at short TE, the tail of this residual water may overlap with the baseline of macromolecule/lipids and thus, pose problems for accurate quantification. As a solution, the Hankel Lanczos Singular Value Decomposition (HLSVD) method proposed by (Pijnappel et al., 1992) parametrizes

the MR signals as a sum of complex-damped exponentials. Extensions of this method for quantification and peak suppression have been successfully applied to MR signals (Chen et al., 2004; Laudadio et al., 2004). Alternative to HLSVD, other filtering approaches have also been used for this purpose (Antoine et al., 2000; Sundin et al., 1999). Additional to the residual water, other unwanted resonances (*e.g.*, reference peaks from *in vitro* phantom solutions) may also need to be suppressed from the spectrum (Cabanes et al., 2001).

3. Quantification

Several quantification methods have been developed in the time and the frequency domain to determine metabolite concentrations. Thus, depending on the nuclei, the complexity of the signal and the *prior* information available, MR signals can be quantified with the methods listed below. An extended review of time- and frequency domain methods has been given in (Mierisová & Ala-Korpela, 2001; Vanhamme et al., 2001) and more recently in (Poullet et al., 2008).

- Time- and frequency domain fitting using a linear combination of individual peaks/profiles to fit the spectra QUEST (Ratiney et al., 2004), AQSES (Poullet et al., 2007) LCModel (Provencher, 1993; 2001)
- Time-domain estimation of parameters using *prior knowledge* (Soher et al., 1998; Young et al., 1998), AMARES (Vanhamme et al., 1997)
- Time-domain non-iterative fitting methods such as HLSVD (Barkhuijsen et al., 1987; Chen et al., 1996; Dologlou et al., 1998; Laudadio et al., 2002; Pijnappel et al., 1992; van den Boogaart, 1997)
- Iterative time- and frequency domain fitting (Slotboom et al., 1998)
- Semi-parametric fitting (Elster et al., 2005)
- Time-domain variable projection (VARPRO) (Cavassila et al., 1999; van der Veen et al., 1988)
- Time domain fitting of one peak at a time and wavelet modeling for the baseline (Dong et al., 2006; Romano et al., 2002)
- Constrained least squares (TARQUIN) (Reynolds et al., 2006; Wilson et al., 2011)
- Genetic algorithms (Metzger et al., 1996)
- Fast Padé Transform (Belkić & Belkić, 2006)
- Artificial Neural Networks (Bhat et al., 2006; Hiltunen et al., 2002)
- Sparse representation (Guo et al., 2010)
- Circular fitting (Gabr et al., 2006)
- Principal Component Analysis (PCA), Independent Component Analysis (ICA) (Hao et al., 2009; Stoyanova & Brown, 2001)

3.1 Automated Quantification of Short echo time MRS signals (AQSES)

We present in more details the method AQSES, which will be used in the next sections to illustrate several recent improvements in the field of MRS(I) signal processing. This time-domain quantification method has been especially developed for short TE MRS signals, where a mathematical model fits to a basis set of predefined metabolite profiles. From this fit, metabolite amplitudes are obtained, which represent the weighting coefficients of a linear combination of corrected metabolite profiles with Lorentzian lineshapes used for quantification. Finally, these values are proportional to the concentrations of all estimated metabolites. AQSES is available in the Java open source software AQSES GUI (De Neuter et al., 2007; Poullet et al., 2007), as a quantification method inside the Matlab® graphical user interface SPID (Poullet, 2008) and as a plug-in in the jMRUI software package (version 4.1) (Stefan et al., 2009). Fig. 2 shows the results window for a quantification made in SPID.

The model describing a short TE *in vivo* time-domain MRS signal $y(t)$ as a combination of several metabolite profiles is:

$$y(t) = \sum_{k=1}^{K} a_k e^{(j\phi_k)} e^{(-d_k t + 2\pi j f_k t)} v_k(t) + B(t) + w(t) + \epsilon(t) \tag{1}$$

where K is the number of metabolites ($k = 1, \ldots, K$), $v_k(t)$ the metabolite profile in the basis set measured as individual phantoms or simulated using quantum mechanics, a_k the amplitudes, ϕ_k the phase shifts, d_k the damping corrections, f_k the frequency shifts due to field inhomogeneity, $j = \sqrt{-1}$, $B(t)$ is the baseline due to macromolecule/lipid contamination (in AQSES it is fitted via nonparametric modeling using a basis of splines (Eilers & Marx, 1996)), $w(t)$ the water resonance (filtered either before quantification as explained in section 3.2.1, or during quantification as in (Sundin et al., 1999)) and $\epsilon(t)$ denotes white noise with standard deviation σ.

In order to assess quantification results, the Cramér-Rao lower bounds (CRLB) (Cavassila et al., 2001) are computed to provide an indication about the uncertainty and reliability of the estimated amplitudes (concentrations). Small CRLB values may (but not necessarily) indicate good parameter estimates and are proportional to the variance of the residue obtained from subtracting the fitted signal and the baseline from the original signal. Thus, acceptable CRLB should normally be below 40%.

3.2 Methods for quantification improvement

Although the quantification of *in vivo* MRS signals can often be reliably done using model (1) in AQSES, several issues appear when high field, short TE signals or multi-voxel MRSI data are being quantified. In this section, we present several quantification improvement methods implemented in AQSES (Croitor Sava, 2011; Osorio-Garcia, 2011). Whereas the filter of residual water is performed as a preprocessing step, the lineshape and baseline estimation methods are included inside the quantification method. Finally, a modified version of AQSES for MRSI data, which includes spatial knowledge is presented.

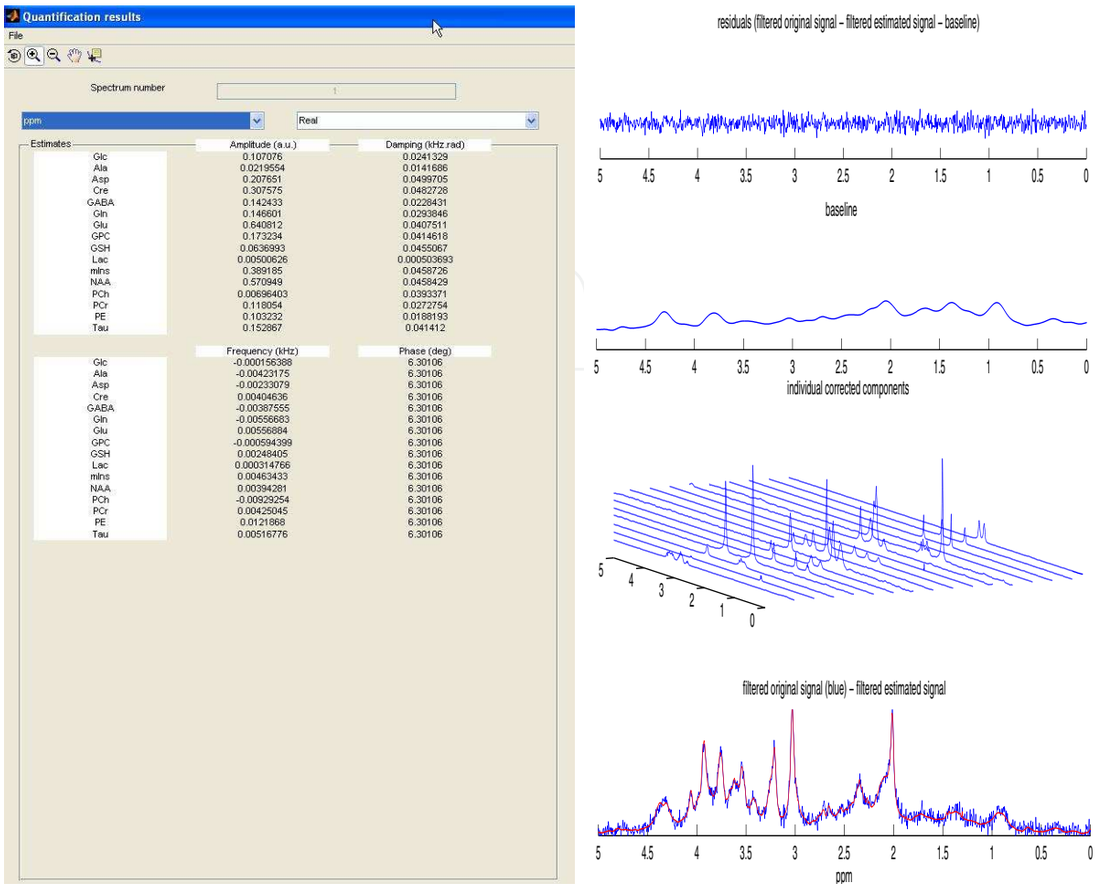

Fig. 2. Quantification results window for AQSES in SPID (left side) of an *in vivo* ^{1}H MRS signal from mouse brain acquired with a 9.4 T Bruker Biospec small animal MR scanner (Bruker BioSpin MRI, Ettlingen, Germany) with acquisition parameters: PRESS sequence, TR=4 s, TE=12 ms, SW=4 KHz, NDP=2048 points and 256 averages, volume of interest (VOI)= $3 \times 1.75 \times 1.75\ mm^3$. The basis set of 16 metabolites used for quantification was measured *in vitro*. Right: plots of residue, splines baseline, estimated metabolites and original with estimated signal.

3.2.1 Filtering of residual water

As described in section 2.2, the water component ($w(t)$ from Eq.(1)) can be filtered using HLSVD, however, appropriate filtering of this resonance in the case of distorted signals is often inaccurate. When HLSVD with one component (*i.e.*, a model order $K = 1$) is used to fit one non-Lorentzian peak, the result obtained by subtracting that modeled peak from the original signal produces a non-flat residual. In an ideal case, only white noise should be left in the residual.

The state-of-the-art methods proposed for determination of an optimal model order K in order to provide a reliable water peak removal have been described and studied on simulated, noiseless or non-overlapping peaks (Cabanes et al., 2001; Hu et al., 2010; Lin et al., 1997; Papy et al., 2007; Van Huffel & Vandewalle, 1991). For instance, (Cabanes et al., 2001) presented a method for optimal residual water removal of *in vivo* ^{1}H MRS signals of

human brain using HLSVD with a model order of 25 ($K = 25$). Nevertheless, suppression of unwanted resonances of *in vivo* MRS signal using HLSVD may require more than 25 components. In fact, it is certain that a higher model order may better fit one non-Lorentzian peak. In such cases, the model order in HLSVD can be overestimated to adequately fit the experimental signal with distorted shape. Finally, all components encountered in the selected filtering region are suppressed without affecting the other resonances.

Therefore, we present a heuristic approach to estimate the model order by overestimating the number of components in HLSVD (Osorio-Garcia, 2011). In this chapter, we use the Lanczos algorithm with partial reorthogonalization, HLSVD-PRO (Laudadio et al., 2004). First, the tail of the time domain signal is truncated in order to obtain by Fourier transformation a spectrum with lower, but still adequate, spectral resolution; this truncation starts at the point at which the FID completely decays into the noise. Then, the signal is transformed to the frequency domain and an estimated number for the model order is obtained by counting the number of spectral points larger in absolute value than a noise-related threshold. We illustrate in Fig. 3 to 6 good peak suppression results on short TE *in vivo* and *in vitro* ^{1}H MRS signals, as follows:

- **1.5 T signals**. Filtering of residual water and reference peaks for an *in vivo* (normal human brain) and an *in vitro* (NAA) MRS signal obtained at 1.5 T was done by suppressing all peaks in the frequency region outside the intervals [0 ppm, 4.3 ppm] and [1 ppm, 4.44 ppm], respectively. For the *in vivo* signal in Fig. 3, results for $K = 25$ and K overestimated ($K = 44$) show a good water suppression, but the water region is flatter when $K = 44$. Fig. 4 illustrates the incomplete filtering of the reference peaks at 0 ppm and 8.4 ppm corresponding to solvents added to the NAA phantom solution when $K = 25$, but this is not the case when K is overestimated, thus, $K = 309$.
- **9.4 T signals**. Filtering of residual water and reference peaks for an *in vivo* (mouse brain) and an *in vitro* (Glucose (Glc)) MRS signal obtained at 9.4 T was done by suppressing all peaks in the frequency region outside the intervals [0 ppm, 4.3 ppm] and [2.95 ppm, 4.44 ppm], respectively. A residual reference peak located at 2.8 ppm contained in the *in vitro* signal could only be suppressed when K was overestimated. Figures 5 and 6 show the results for both signals.

3.2.2 Lineshape estimation

The metabolite profiles used for quantification have ideally a Lorentzian shape, however, the lineshape of the metabolite resonances in an *in vivo* signal might be distorted. We aim to estimate the lineshape distortion from the *in vivo* signal and impose the same distortion to each individual metabolite to ensure the same lineshape in both the *in vivo* and the model spectra. Here, we present a method (AQSES Lineshape) to estimate a common lineshape which has been successfully used in simulated, *in vitro* and *in vivo* signals (Osorio-Garcia et al., 2011; Sima et al., 2009).

In the presence of magnetic field inhomogeneities due to field perturbations or tissue heterogeneities, the symmetry and linewidth of the lineshapes are disturbed. Therefore, the fitting of the MR signal using an ideal lineshape (*e.g.*, Lorentzian, Gaussian or Voigt) becomes unreliable. Although some preprocessing methods can correct lineshape distortions, the use of a separate reference acquisition signal or a well-separated reference peak may limit their applicability.

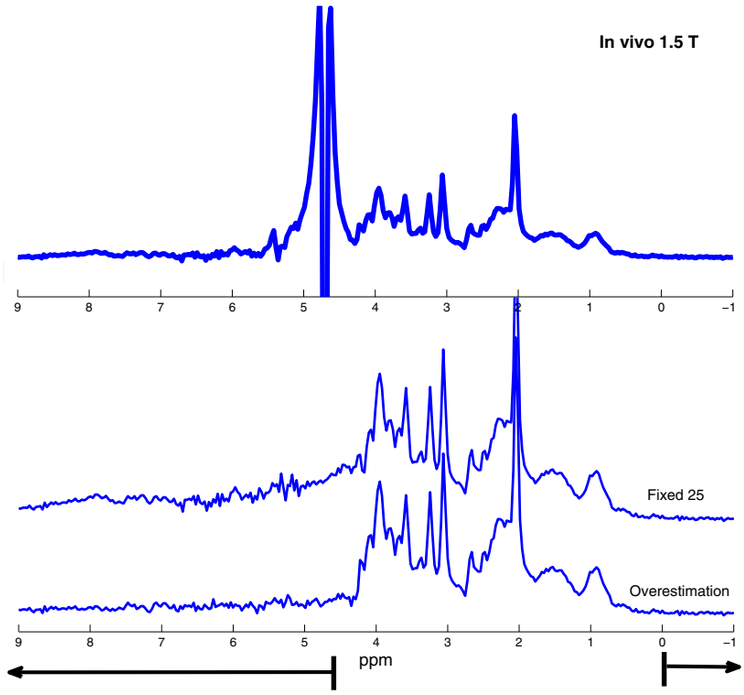

Fig. 3. Top: Real part of the spectrum of an *in vivo* MRS signal measured at 1.5 T with acquisition parameters: Philips scanner, PRESS sequence, TR=6 s, TE=23 ms, SW=1 KHz, NDP=512 points and 64 averages. Bottom: filtered signals using HLSVD-PRO with the model orders of $K = 25$ and overestimated as $K = 44$. All modeled peaks in the frequency region outside the interval [0 ppm, 4.3 ppm] were suppressed.

The lineshape of a peak in the frequency domain is determined by the decay function (damping) of the time domain signal. Self-deconvolution methods make use of the fact that within a measurement the most important factor that determines the decay rate is the local field heterogeneity, thus, all metabolites are distorted in the same way and therefore, a common lineshape can be estimated. Nevertheless, the computation of this lineshape produces a noisy function that needs to be converted into a smooth function. Methods in the literature differ in the approaches used for smoothing this noisy function. Here, we present a lineshape estimation method for correcting lineshape distortions during quantification with AQSES, where the exponential dampings $e^{(-d_k t)}$ in Eq.(1) are replaced by the common factor $g(t)$ of arbitrary shape:

$$y(t) = g(t) \sum_{k=1}^{K} a_k e^{(j\phi_k)} e^{(2\pi j f_k t)} v_k(t) + B(t) + \epsilon(t) \tag{2}$$

The AQSES Lineshape algorithm for lineshape estimation is described below.

Step 1. Initial fitting. Quantification of the signal assuming a Lorentzian lineshape to extract the spectral parameters: amplitudes, frequencies, phases and dampings using the model in Eq. (1). Then, the signal is reconstructed from the estimated spectral parameters without considering the damping estimates.

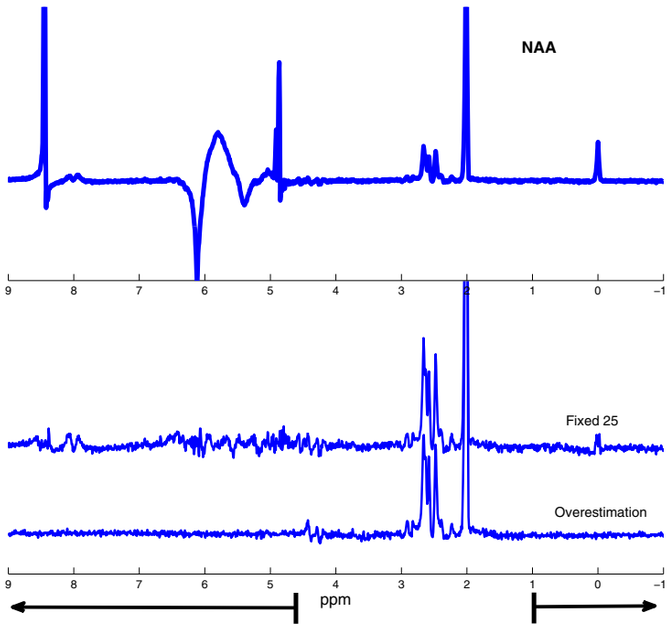

Fig. 4. Top: Real part of the spectrum of *in vitro* NAA measured at 1.5 T with acquisition parameters: Philips scanner, PRESS sequence, TR=6 s, TE=23 ms, SW=1 KHz, NDP=2048 points and 128 averages. Bottom: filtered signals using HLSVD-PRO with the model orders of $K = 25$ and overestimated as $K = 309$. All modeled peaks in the frequency region outside the interval [1 ppm, 4.44 ppm] were suppressed. Residual resonances are visible for $K = 25$ in the water and reference peak regions, *i.e.*, 4.7 ppm, 0 ppm and 8.44 ppm.

Step 2. Damping estimation. Computation of the damping function $g(t)$ as:

$$g(t) = \frac{y(t) - B(t)}{\sum_{k=1}^{K} a_k e^{(j\phi_k)} e^{(2\pi j f_k t)} v_k(t)} \tag{3}$$

where $y(t)$ is the experimental signal, $B(t)$ is the current baseline estimate, K is the number of metabolites, $v_k(t)$ the metabolite signal k in the basis set, and the amplitudes a_k, frequency shifts f_k and phase shift ϕ_k are estimated from a previous AQSES iteration from **Step 1** or **Step 4**.

Step 3. Smoothing. Outliers caused by numerical instability and division by small numbers are reduced using local regression (LOESS). This method assigns lower weight to outliers in the regression (Cleveland, 1979) and allows a robust smoothing. (See Fig. 7)

Step 4. Estimate. Spectral analysis is carried out again after point-wise multiplying the original metabolite basis set with the new smoothed function $g(t)$ from **Step 3**.

Steps 2-4 are repeated until a residual smaller than a chosen threshold is obtained or a convergence of amplitude estimates is reached.

Results of the lineshape estimation are shown below.

- **Simulated signals.** The simulated MRS signals were generated as a linear combination of 7 *in vitro* measured metabolites: Alanine (Ala), Creatine (Cr), Glutamine (Gln), Glutamate (Glu), Lactate (Lac), N-Acetyl-Aspartate (NAA), and Taurine (Tau). Then a distortion

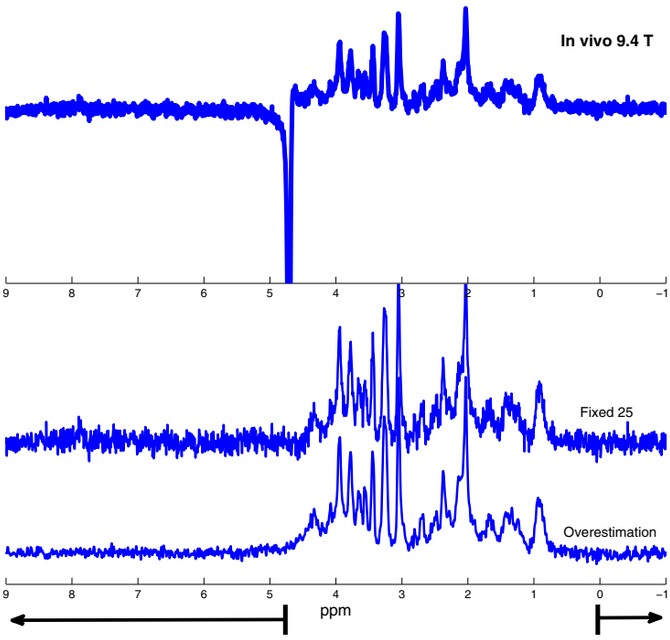

Fig. 5. Top: Real part of the spectrum of an *in vivo* MRS signal measured at 9.4 T with acquisition parameters: PRESS sequence with implemented pre-delay OVS as well as the water suppression method VAPOR, FASTMAP shimming correction, TR=4 s, TE=12 ms, SW=4 KHz, 2048 points and 256 averages. Bottom: Filtered signals with the model orders of $K = 25$ and overestimated as $K = 134$. All modeled peaks in the frequency region outside the interval [0 ppm,4.3 ppm] were suppressed.

was included to simulate a damping different from the ideal Lorentzian. Fig. 8 shows the quantification results obtained for a set of simulated signals with triangular and eddy current distortions having small and large dampings. The top row shows the fits with AQSES and AQSES Lineshape with the corresponding residuals when simulating the signals with a small (left) and a large (right) damping. The residual corresponding to AQSES contains some patterns corresponding to metabolite contributions that were not correctly quantified due to the Lorentzian lineshape model, whereas the residuals corresponding to AQSES Lineshape show a nearly flat line containing white noise that may be attributed to the estimated lineshape model. At the bottom of each plot, the amplitude estimates using AQSES and AQSES Lineshape are shown.

- ***In vitro* signals.** An *in vitro* signal containing Ala, Cr, Gln, Glu, Lac, NAA and Tau was acquired using the default shimming technique with linewidth=1.36 Hz and SNR=22. The magnetic field was afterwards intentionally distorted by mis-setting the shim current of the X coil in order to simulate lineshape distortions caused by incorrect shimming; two distorted signals were then acquired. Results of quantification of *in vitro* signals are shown in Fig. 9. The undistorted *in vitro* signal is fitted identically by AQSES and AQSES Lineshape, *i.e.*, AQSES Lineshape reports convergence after the first iteration (results not shown). For the distorted signals, the resonances of Cr at 3 ppm and 3.9 ppm and the one from NAA at 2 ppm are not very well fitted with AQSES, while AQSES Lineshape is able to fit these peaks. This is due to the fact that the lineshape distortions have a shape different from the typical Lorentzian type considered by AQSES.

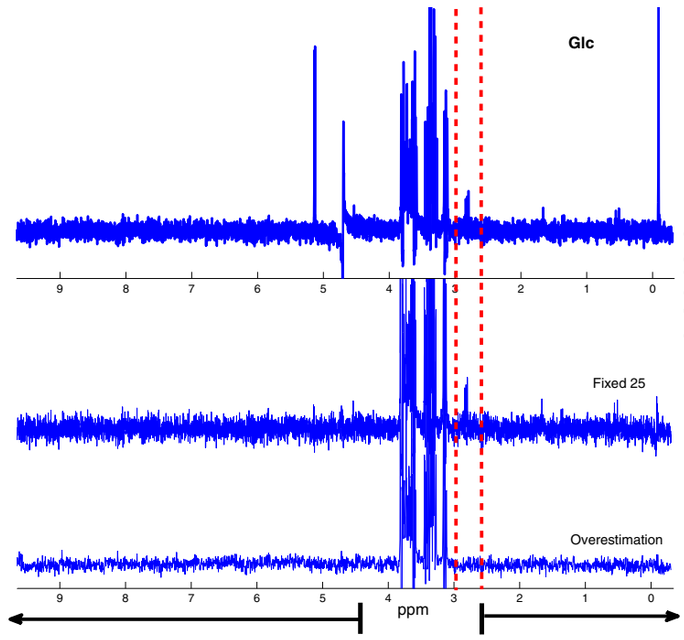

Fig. 6. Top: Real part of the spectrum of *in vitro* Glc measured at 9.4 T with acquisition parameters: PRESS sequence with implemented pre-delay OVS as well as the water suppression method VAPOR, FASTMAP shimming correction, TR=4 s, TE=12 ms, SW=4 KHz, 6144 points and 64 averages. Bottom: filtered signal with the model orders of $K = 25$ and overestimated as $K = 126$. All modeled peaks in the frequency region outside the interval [2.95 ppm,4.44 ppm] were suppressed. Residual resonances are visible at the region around 2.8 ppm (between the two vertical dashed lines).

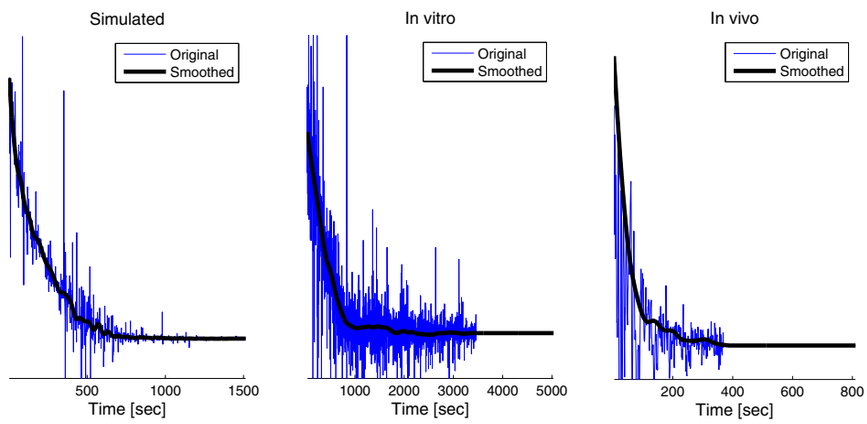

Fig. 7. Time domain signal of the resulting lineshape for simulated (left), *in vitro* (middle) and *in vivo* (right) signals. The signal labeled as 'Original' corresponds to the $g(t)$ function calculated with the ratio formula in Eq.(3) and the smoothed signal is its final denoised version after convergence.

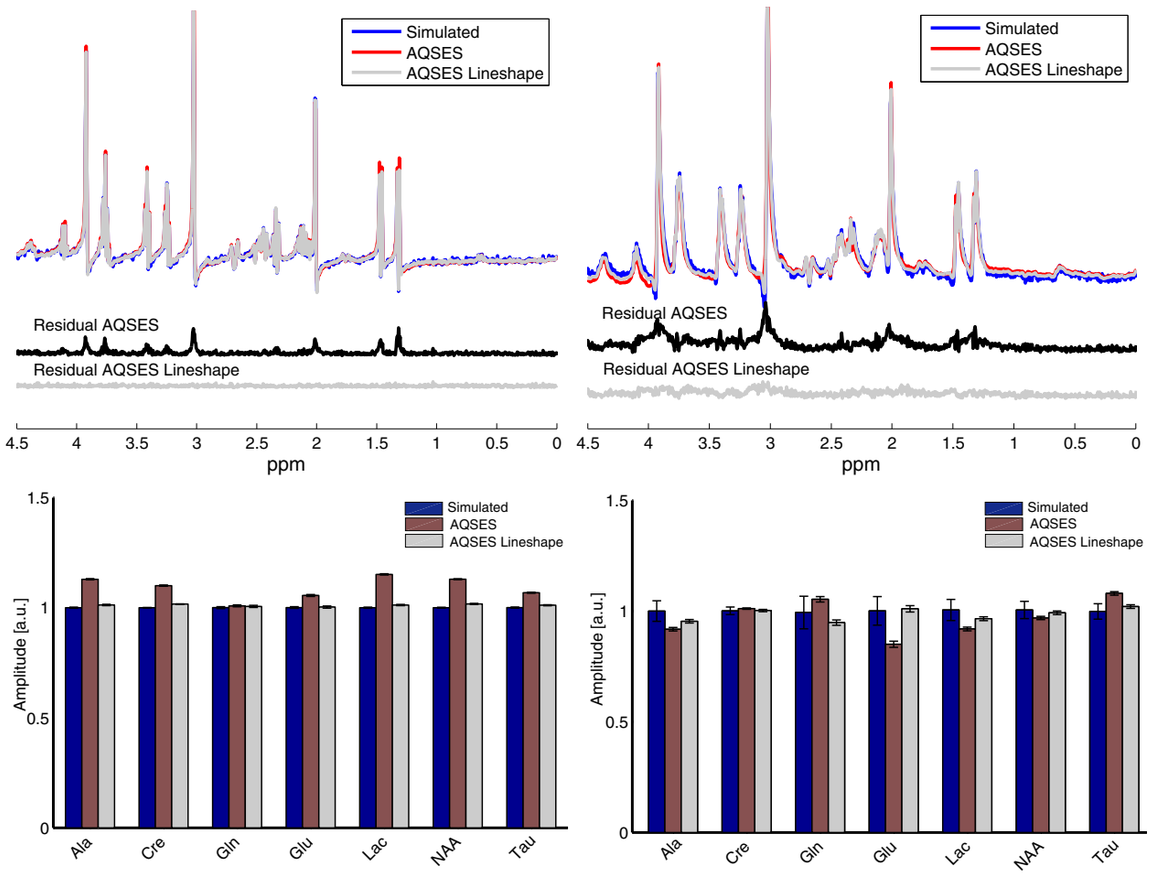

Fig. 8. Simulated MRS signals with lineshape distortions and the corresponding quantification results. These signals were obtained as the linear combination of 7 metabolites (Ala, Cr, Gln, Glu, Lac, NAA, and Tau) measured *in vitro* at 9.4 T with acquisition parameters: PRESS sequence, TR=8 s, TE=20 ms, SW=4 KHz and NDP=2048 points and 64 averages. Top left: small damping (to simulate *in vitro* signals). Top right: large damping (to simulate *in vivo* signals). The bottom plots represent the amplitude estimates for the corresponding simulated signals using AQSES and AQSES Lineshape.

- ***In vivo* signals.** An *in vivo* signal was acquired using the default shimming technique. Then, after modifying the first and second order shim coils X and Z^2, two mis-shimmed signals were also acquired. The undistorted *in vivo* signal was fitted similarly by AQSES and AQSES Lineshape, *i.e.*, AQSES Lineshape reports convergence after the first iteration (results not shown). Results of quantification for the two distorted *in vivo* signals are shown in Fig. 10.

3.2.3 Baseline estimation

The contribution from macromolecules and lipids may vary depending on the anatomical region or due to disease (tumor or metabolic disease), providing potentially useful diagnostic information, but also creating a sort of baseline in the spectra. As a consequence, some of these macromolecule/lipid resonances also overlap with metabolite peaks and it is necessary to account for these contributions during the quantification. Therefore, several baseline methods

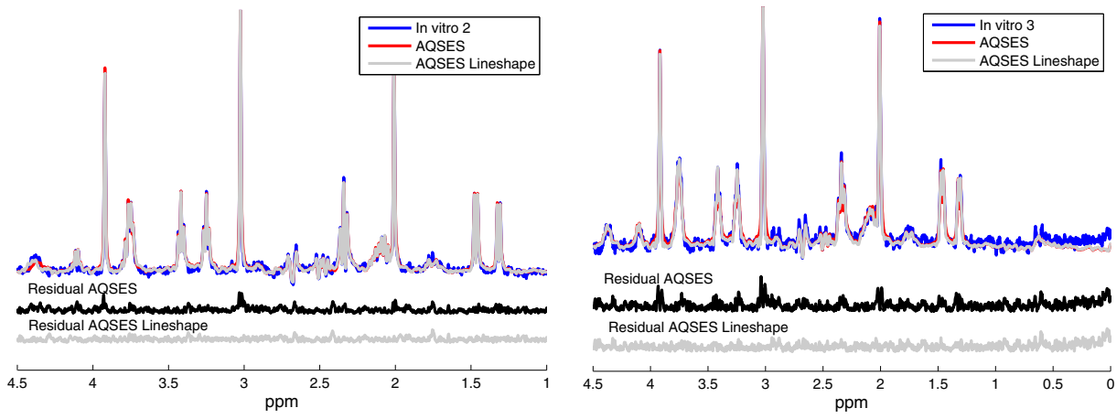

Fig. 9. Spectra of *in vitro* MRS signals measured with a Bruker scanner at 9.4 T containing 7 metabolites: Ala, Cr, Gln, Glu, Lac, NAA, and Tau. Acquisition parameters: PRESS sequence, TR=8 s, TE=20 ms, SW=4 KHz and NDP=2048 points and 128 averages. Two distorted signals were acquired by mis-setting the shim current of the X coil, Left: 'in vitro 2' with linewidth=3.92 Hz and SNR=20. Right: 'in vitro 3' with linewidth=6.52 Hz and SNR=18. Both were quantified by AQSES and AQSES Lineshape.

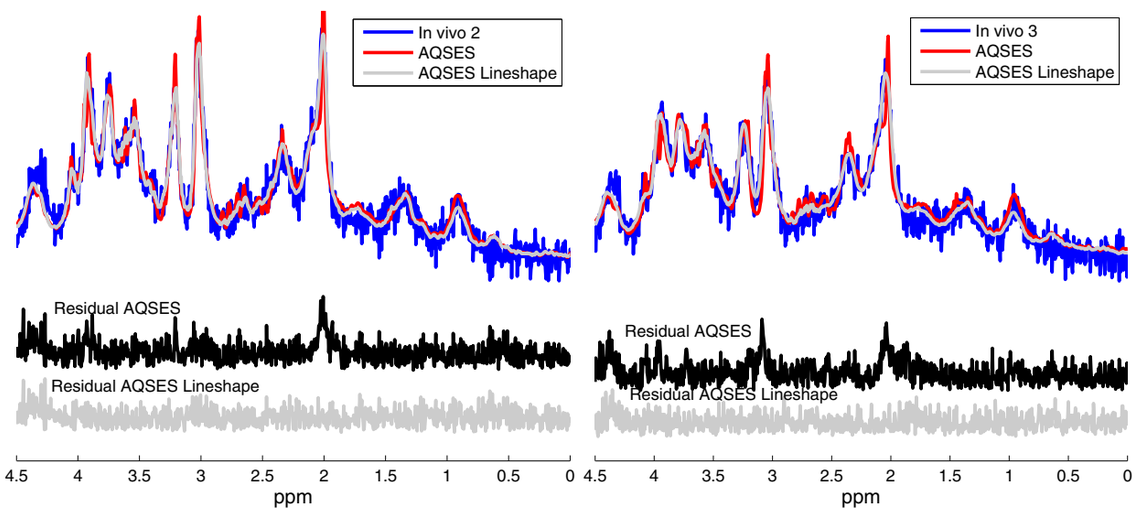

Fig. 10. Rat brain *in vivo* spectra from the right hemisphere of the thalamus measured with a Bruker scanner at 9.4 T with acquisition parameters: PRESS sequence, TR=8 s, TE=20 ms, SW=4 KHz, NDP=2048 points and 128 averages. 'In vivo 2' and 'in vivo 3' were acquired by mis-setting the shimming parameters of the first and second order shim coils X and Z^2. The linewidth for these signals was 27.8 Hz and 39.69 Hz, respectively with SNR=20. Both were quantified by AQSES and AQSES Lineshape.

have been developed based on advanced acquisition techniques using inversion recovery (*i.e.*, metabolite-nulled spectrum) (Cudalbu et al., 2009; Kunz et al., 2010; Mlynárik et al., 2008; Pfeuffer et al., 1999), parametric (Bartha et al., 1999; Seeger et al., 2003) and non-parametric estimation methods (Poullet et al., 2007; Provencher, 2001; Ratiney et al., 2004). Fig. 11 shows an *in vivo* MRS signal from a mouse brain obtained at 9.4 T and the macromolecule/lipid baseline obtained via inversion recovery.

Here, we present a method that extracts characteristic information from a set of inversion recovery MM signals. Thus, individual macromolecule/lipid components are computed and included in the metabolite basis set used in the AQSES quantification method.

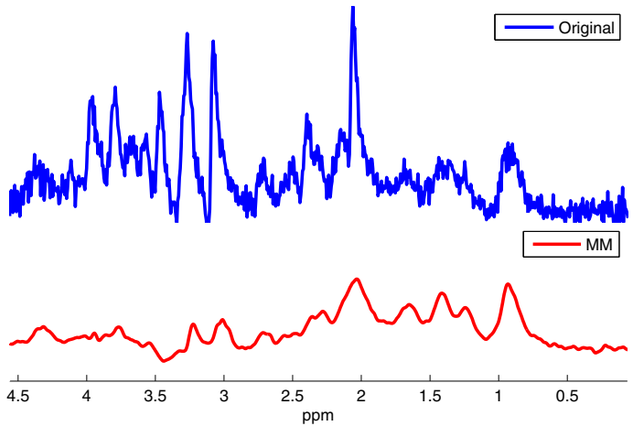

Fig. 11. Real part of the spectrum of an *in vivo* MRS signal and an MM signal obtained from a mouse brain. 'Original' acquisition parameters: Bruker 9.4 T scanner, PRESS sequence, TR=4 s, TE=12 ms, SW=4 KHz and 256 averages. 'MM' acquisition parameters: Bruker 9.4 T scanner, TI=800 ms, TR=3 s, NDP=2048 points and 1024 averages.

Characterization of the macromolecular baseline was addressed by modeling m previously identified profiles shown in Fig. 12 left. Thus, a set of 10 inversion recovery signals was first measured and m individual lipid and macromolecular peaks were identified as *prior knowledge*. These resonances were observed at frequency locations around: 0.89 (MM1), 1.20 (MM2), 1.36 (MM3), 1.63 (MM4), 2.02 (MM5), 2.29 (MM6), 2.65 (MM7), 3.03 (MM8), 3.21 (MM9), 3.75 (MM10), and 4.31 ppm (MM11). The spectral fitting method AMARES (Vanhamme et al., 1997) in jMRUI (Stefan et al., 2009) was used to quantify the set of inversion recovery signals as a sum of 11 damped sinusoids and the mean of amplitudes, frequency locations and linewidths were used to create the individual MM resonances shown in Fig. 12 right. The final MM components are included in the basis set of AQSES subject to small parameter variations.

When lineshape and baseline estimations are considered in the quantification, the model in Eq. (3) changes and $g(t)$ is estimated as:

$$g(t) = \frac{y(t) - B(t)}{\sum_{k=1}^{K} a_k e^{(j\phi_k)} e^{(2\pi j f_k t)} v_k(t) + \sum_{i=1}^{m} \tilde{a}_i e^{(j\tilde{\phi}_i)} e^{(2\pi j \tilde{f}_i t)} MM_i(t)} \tag{4}$$

where $y(t)$ is the experimental signal, $B(t)$ is the non-parametric (spline) baseline from the previous iteration, $MM_i(t)$ is the set of modeled profiles, K is the number of metabolites, $v_k(t)$

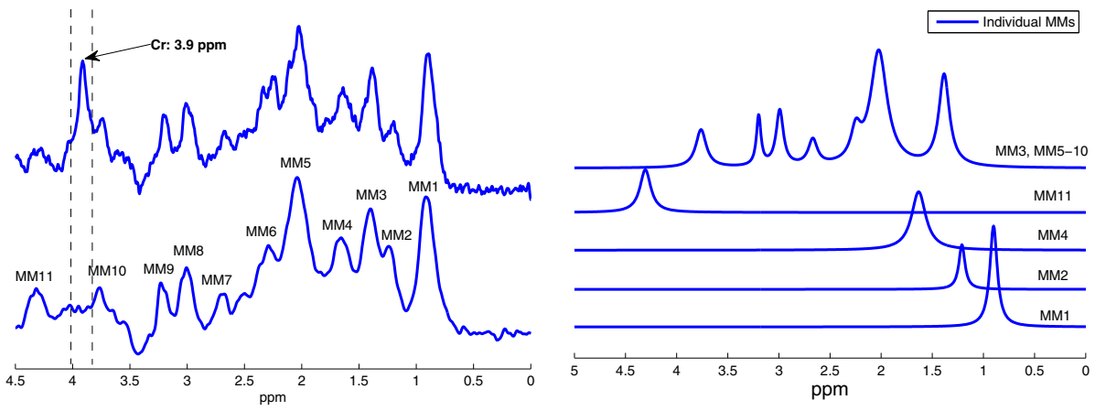

Fig. 12. **Left:** Real part of an *in vivo* metabolite-nulled MM spectrum acquired with a Bruker scanner at 9.4 T with acquisition parameters: TI=800 ms, TR=3 s, NDP=2048 points and 1024 averages. Spectra were post-processed with a 15 Hz Lorentzian line broadening. Due to a shorter T_1, the marked (Cr + PCr) resonance at 3.9 ppm was not completely minimized, therefore this peak was filtered out using HLSVD-PRO (top curve). Macromolecular resonances are labeled as MM from 1 until 11 at the following central frequencies: 0.89, 1.20, 1.36, 1.63, 2.02, 2.29, 2.65, 3.03, 3.21, 3.75, 4.31 ppm; the mean of 10 filtered MM signals is shown in the bottom curve. **Right:** Real part of the MM spectrum obtained with AMARES using *prior knowledge* from the measured inversion recovery signals. This plot shows the individual MMs computed based on the mean of the AMARES estimates of all measured MMs. Small variations are expected for different signals which are then corrected by AQSES.

the metabolite signal k in the basis set, and the amplitudes a_k, $\tilde{a}_i$, frequency shifts f_k, $\tilde{f}_i$ and phase shift ϕ_k, $\tilde{\phi}_i$ are estimated from the previous iteration of the AQSES Lineshape algorithm.

To avoid mis-quantification due to overlapping of MM resonances with metabolites, we combined MM3 with MM5-MM11 to obtain a single profile of seven resonances located in the region between 2 ppm - 4.1 ppm where all important metabolites are resonating. Fig. 13 shows the results of fitting using the mean of inversion recovery measured baselines and the mean of individual MMs obtained with AMARES (*i.e.*, five MM profiles).

3.2.4 Inclusion of spatial constraints in MRSI quantification

Magnetic Resonance Spectroscopic Imaging (MRSI) provides MR spectra from multiple adjacent voxels within a body volume represented as a 2 or 3 dimensional matrix, allowing measurement of the distribution of metabolites over this volume. Commonly, for estimating the metabolite concentrations, the signals within an MRSI grid are analyzed on a single voxel basis by quantifying each signal individually. To this aim, methods such as QUEST (Ratiney et al., 2005), AQSES (Poullet et al., 2007) or AMARES (Vanhamme et al., 1999) may be considered (the list can be extended, see the methods listed at the beginning of section 3). Compared with *in vitro*, *ex vivo* and single voxel *in vivo* MRS signals, *in vivo* MRSI data have a lower quality due to the spatial/spectral trade-off. Moreover, the magnetic field inhomogeneities, relatively low signal-to-noise ratio (SNR) and physiological motion that might appear during an MRSI acquisition compromise the spectral resolution and lead to strongly overlapping metabolite peaks. Therefore, quantifying metabolites within MRSI

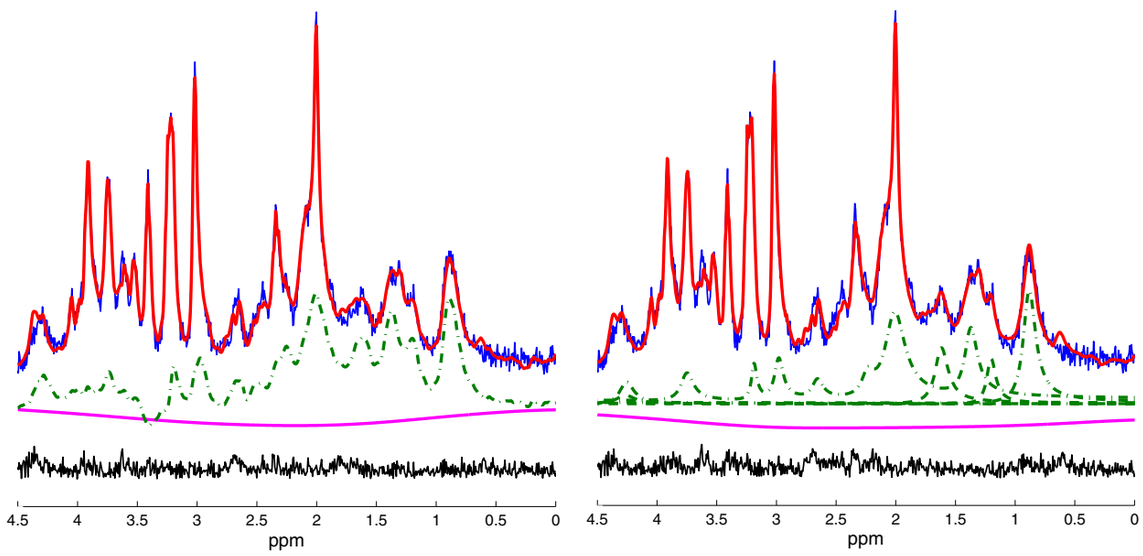

Fig. 13. AQSES fit for the mean spectra of short TE ^{1}H MRS *in vivo* from mouse brains. Real part of the *in vivo* spectrum (noisy signal) together with the fit using AQSES (bold line on top of the signal), MM (dash-dotted curve below the signal), spline baseline (smooth curve below the MM signal) and the residual (noisy line beneath). Quantification was made accounting for the baseline in two ways: (i) considering a metabolite-nulled signal computed as the mean of all measured signals (left) and (ii) considering 5 MM profiles obtained via AMARES (right). Additionally, a very smooth splines function was used to fit any broadening of the baseline.

data on a voxel-by-voxel basis can suffer from accuracy limitations that are inherent to maximum likelihood estimation, and, moreover, it can be prone to faulty convergence to local minima. Since MRSI provides spatial knowledge, in order to improve quantification results, and thus, metabolite estimates in MRSI data, a new metabolite quantification method, in which the available spatial information is exploited, has been proposed. The method, called AQSES-MRSI, is a modified version of AQSES for MRSI data (Croitor Sava et al., 2011).

AQSES-MRSI starts by individually fitting each signal in the grid using nonlinear least squares (Poullet et al., 2007; Sima & Van Huffel, 2007) to extract the spectral parameters, frequencies and dampings, from each voxel which will be further used as *prior knowledge*. Then, for the quantification of each voxel c within the MRSI grid, spatial information is taken into account in more steps. Moreover, several sweeps are performed through the grid and at each run some hyper-parameters may be tuned. Firstly, the starting values for the nonlinear parameters, θ_c (vector containing damping corrections and frequency shifts for voxel c) are optimized by setting them to the median of the parameter values from the considered neighbors $\theta_s (s = 1, \ldots, S$, where S is the total number of voxels in the considered neighborhood). Secondly, optimized bounds on the parameters' variability are computed so that the parameters of the neighboring voxels do not present a high variability. Thirdly, a penalty term that promotes a spatially smooth spectral parameter map for the frequency shifts and damping corrections are imposed, while allowing complete freedom to the metabolite amplitudes. The weight on the smoothness of individual parameters is adjustable:

$$\min_{\theta_c} \frac{1}{N} \sum_{t=t_0}^{t_{N-1}} \left| y_c(t) - \hat{y}_c(t, \theta_c) \right|^2 + \sigma^2 \sum_{\theta_c \neq \theta_s} \varepsilon_s \beta_{cs} \left\| W(\theta_c - \theta_s) \right\|_2^2 \quad (5)$$

where the signal $y_c(t)$ corresponds to voxel c in the grid and the model $\hat{y}_c(t, \theta_c)$ is considered as a weighted sum of metabolite signals with nonlinear corrections θ_c, similarly to the model in Eq. (1). The second term, called penalty term, encourages a smooth solution for the problem. ε_s accounts for the trade-off between an optimal fitting of the current signal and the penalty, σ^2 is an estimate of the noise variance computed from the tail of the signal in time domain in voxel c, β_{cs} is a weighting scalar which gives the influence of the parameters θ_s on the parameters θ_c (as described below), W is a diagonal weighting matrix, with $W \in R^{Km \times Km}$, which accounts for the scale differences between parameters, where K is the number of metabolite profiles and m is the number of parameters per metabolite.

AQSES-MRSI's performance on simulated MRSI data with several types of disturbances and on short echo time *in vivo* proton MRSI data showed improved metabolites estimates compared to quantification of each voxel signal individually, see Fig. 14 and 15. With

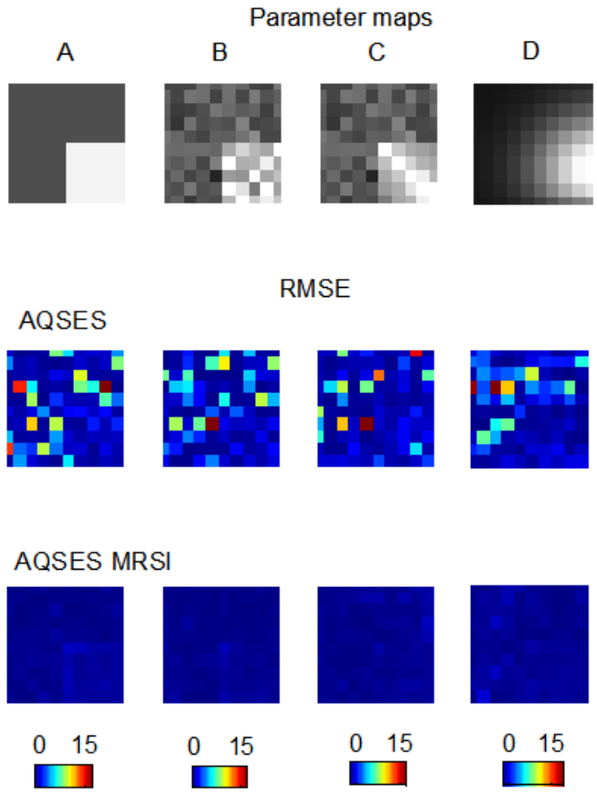

Fig. 14. First row: simulated MRSI grids with different parameter maps: A-D. 2nd and 3rd row illustrate color maps with the values of the error in estimating the metabolite concentrations, computed as a root mean square error (RMSE computed as in (Croitor Sava et al., 2011)), for each voxel for AQSES and AQSES-MRSI, respectively.

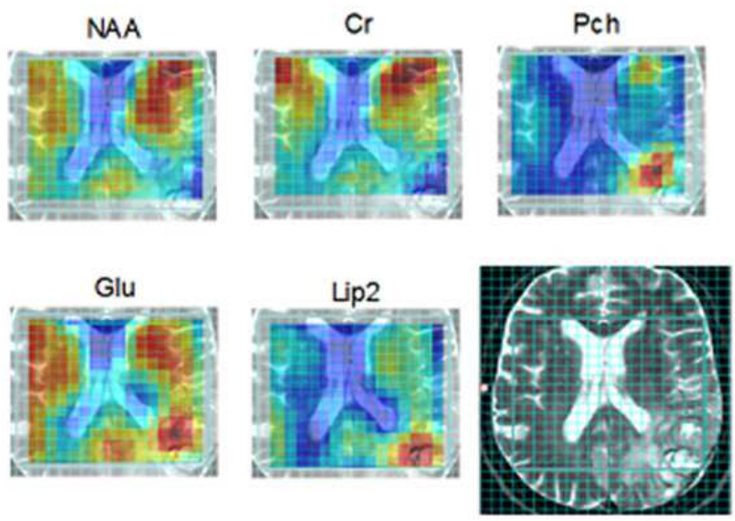

Fig. 15. Metabolic maps obtained after applying AQSES-MRSI. The color scheme is relative to each metabolite. The patient is diagnosed to have glioblastoma tumor (lower right corner of the MRI image).

AQSES-MRSI, overlapping peaks or peaks of compounds present at low concentration can be better resolved than in single-voxel approaches.

Fig. 14 presents four simulated MRSI data sets of 10×10 voxels generated with different levels of inhomogeneities within the parameter maps. 75% of each simulated MRSI grid contains a region with normal-tissue-like spectra and 25% of the grid presents tumor-tissue-like spectra (damping, frequency and amplitude values were set to values corresponding to the signals measured in normal brain and tumor region, respectively). The simulated MRSI signals were obtained as a linear combination of 11 metabolite profiles: NAA, myo-inositol (Myo), Cr, Phosphocholine (PCh), Glu, Lac, Ala, Glc, Tau plus two simulated lipids profiles located at 1.3 ppm (Lip1) and 0.9 ppm (Lip2). These profiles were selected from a measured database acquired with a 1.5 T Philips NT Gyroscan using a PRESS sequence with TE=23 ms, and a PRESS box of $2 \times 2 \times 2$ cm^3. The results illustrated in Fig. 14 show that regardless of the degree of inhomogeneity, AQSES-MRSI outperforms the single voxel approach, AQSES.

Results on an *in vivo* MRSI case (see Fig. 15) show that AQSES-MRSI method provides a much less noisy spatial metabolite distribution compared to single voxel approaches (Croitor Sava et al., 2011). Well-contoured metabolic maps are obtained for all illustrated metabolites. Even metabolites that are difficult to quantify with conventional approaches (see Glu) are well estimated with AQSES-MRSI.

4. Discussion and conclusions

When using HLSVD for filtering the water and unwanted resonances in *in vitro* and *in vivo* MRS(I) signals, the model order plays an important role. Compared to other methods, the overestimation approach is able to suppress distorted lineshape peaks in the presence of low or high SNR. Although we focused on ^{1}H MRS signals, potential implementation with other

nuclei is also feasible. Thus, in MRS signals a good peak suppression is essential to achieve accurate quantification results and is therefore important for a correct usage of the signals.

Even though increasing importance has been given to the lineshape of MR signals, many *in vivo* studies seem to still ignore this problem. For not heavily distorted MRS signals, the Lorentzian lineshape is a good approximation to the shape of the experimental data. However, it is advantageous to rely on a method that takes any shape into account. Therefore, AQSES Lineshape works iteratively and evaluates the performance of tuning a more flexible lineshape starting with the Lorentzian model. As a result, quantification of distorted signals with lineshape estimation showed good quantification results for simulated, *in vitro* and *in vivo* distorted signals.

Although the MM signal acquired by inversion recovery is known to provide a good approximation of the macromolecular contamination, it is also true that it requires a long acquisition time and is not reproducible when the conditions of the region of interest are affected by acquisition problems and various diseases. Moreover, it also contains some unsuppressed metabolites. Nevertheless, the baseline information acquired with this method is a good approximation to the expected MM contributions. Therefore, the presented approach includes *prior knowledge* about the frequency locations, amplitudes and linewidths of individual MM profiles, which are beneficial for the quantification method.

Exploiting spatial *prior knowledge* when analyzing MRSI data has been tackled previously (Bao & Maudsley, 2007; Kelm, 2007; Pels, 2005). In all these approaches a common quantification solution is formulated for the whole MRSI grid. Still, due to the heterogeneity of the tissue that characterizes brain tumors, and to the variations induced by magnetic field inhomogeneities, a common optimization over the whole MRSI array may not always provide satisfactory results. With AQSES-MRSI the bounds on the relevant values of the parameters are iteratively adapted, and/or the parameters of the model function take at each iteration new starting values for each voxel. Such a dynamic approach shows improved quantification results and demonstrates that considering spatial information can improve the estimation of metabolite levels.

5. Acknowledgments

Research supported by: GOA MaNet, CoE EF/05/006 Optimization in Engineering (OPTEC), PFV/10/002 (OPTEC), FWO postdoc grants, IBBT, IUAP P6/04 (DYSCO, 'Dynamical systems, control and optimization', 2007-2011), FAST (FP6-MC-RTN-035801), K.U. Leuven Center of Excellence 'MoSAIC'.

6. References

Antoine, J.-P., Coron, A. & Dereppe, J.-M. (2000). Water peak suppression: Time-frequency vs time-scale approach, *Journal of Magnetic Resonance* 144(2): 189 – 194.

Bao, Y. & Maudsley, A. (2007). Improved reconstruction for MR Spectroscopic Imaging, *IEEE Transactions on Medical Imaging* 26(5): 686 –695.

Barkhuijsen, H., de Beer, R. & van Ormondt, D. (1987). Improved algorithm for noniterative time-domain model fitting to exponentially damped magnetic resonance signals, *Journal of Magnetic Resonance* 73(3): 553 – 557.

Bartha, R., Drost, D. J. & Williamson, P. C. (1999). Factors affecting the quantification of short echo *in vivo* ^{1}H MR spectra: prior knowledge, peak elimination, and filtering, *NMR in Biomedicine* 12(4): 205–216.

Bartha, R., Drost, D., Menon, R. & Williamson, P. (2000). Spectroscopic lineshape correction by QUECC: Combined QUALITY deconvolution and eddy current correction, *Magnetic Resonance in Medicine* 44(4): 641–645.

Behar, K. L. & Ogino, T. (1993). Characterization of macromolecule resonances in the ^{1}H NMR spectrum of rat brain, *Magnetic Resonance in Medicine* 30(1): 38–44.

Belkić, D. & Belkić, K. (2006). *In vivo* Magnetic Resonance Spectroscopy by the fast Padé transform, *Physics in Medicine and Biology* 51(5): 1049.

Bhat, H., Sajja, B. R. & Narayana, P. A. (2006). Fast quantification of proton Magnetic Resonance Spectroscopic Imaging with artificial neural networks, *Journal of Magnetic Resonance* 183(1): 110 – 122.

Blamire, A. M., Rothman, D. L. & Nixon, T. (1996). Dynamic shim updating: A new approach towards optimized whole brain shimming, *Magnetic Resonance in Medicine* 36(1): 159–165.

Cabanes, E., Confort-Gouny, S., Fur, Y. L., Simond, G. & Cozzone, P. J. (2001). Optimization of residual water signal removal by HLSVD on simulated short echo time proton MR spectra of the human brain, *Journal of Magnetic Resonance* 150(2): 116 – 125.

Cavassila, S., Deval, S., Huegen, C., van Ormondt, D. & Graveron-Demilly, D. (1999). The beneficial influence of prior knowledge on the quantitation of *In vivo* Magnetic Resonance Spectroscopy signals, *Investigative Radiology* 34: 242–246.

Cavassila, S., Deval, S., Huegen, C., van Ormondt, D. & Graveron-Demilly, D. (2001). Cramér-Rao bounds: an evaluation tool for quantitation, *NMR in Biomedicine* 14(4): 278–283.

Chang, D., Banack, C. D. & Shah, S. L. (2007). Robust baseline correction algorithm for signal dense NMR spectra, *Journal of Magnetic Resonance* 187(2): 288 – 292.

Chen, H., Van Huffel, S., van Ormondt, D. & de Beer, R. (1996). Parameter estimation with *Prior Knowledge* of known signal poles for the quantification of NMR spectroscopy data in the time domain, *Journal of Magnetic Resonance, Series A* 119(2): 225 – 234.

Chen, J.-H., Sambol, E. B., Kennealey, P. T., O'Connor, R. B., DeCarolis, P. L., Cory, D. G. & Singer, S. (2004). Water suppression without signal loss in HR-MAS ^{1}H NMR of cells and tissues, *Journal of Magnetic Resonance* 171(1): 143 – 150.

Chen, L., Weng, Z., Goh, L. & Garland, M. (2002). An efficient algorithm for automatic phase correction of NMR spectra based on entropy minimization -ACME, *Journal of Magnetic Resonance* 158(1-2): 164 – 168.

Chu, W. C. W., Chik, K., Chan, Y., Yeung, D. K. W., Roebuck, D. J., Howard, R. G., Li, C. & Metreweli, C. (2003). White matter and cerebral metabolite changes in children undergoing treatment for acute lymphoblastic leukemia: Longitudinal study with MR imaging and ^{1}H MR spectroscopy, *Radiology* 229(3): 659–669.

Cleveland, W. S. (1979). Robust locally weighted regression and smoothing scatterplots, *Journal of the American Statistical Association* 74(368): pp. 829–836.

Cobas, J. C., Bernstein, M. A., Martín-Pastor, M. & Tahoces, P. G. (2006). A new general-purpose fully automatic baseline-correction procedure for 1D and 2D NMR data, *Journal of Magnetic Resonance* 183(1): 145 – 151.

Cobas, J. C. & Sardina, F. J. (2003). Nuclear Magnetic Resonance data processing. MestRe-C: A software package for desktop computers, *Concepts in Magnetic Resonance Part A* 19A(2): 80–96.

Croitor Sava, A. R., Sima, D. M., Poullet, J.-B., Wright, A. J., Heerschap, A. & Van Huffel, S. (2011). Exploiting spatial information to estimate metabolite levels in two-dimensional MRSI of heterogeneous brain lesions, *NMR in Biomedicine* 24(7): 824–835.

Croitor Sava, A. R. (2011). *Signal processing and classification for Magnetic Resonance Spectroscopy with clinical applications*, PhD thesis.

Cudalbu, C., Mlynárik, V., Xin, L. & Gruetter, R. (2009). Quantification of *in vivo* short echo-time proton magnetic resonance spectra at 14.1 T using two different approaches of modelling the macromolecule spectrum, *Measurement Science and Technology* 20(10): 104034 (7pp).

de Graaf, A. A., van Dijk, J. E. & BoéE, W. M. M. J. (1990). Quality: quantification improvement by converting lineshapes to the Lorentzian type, *Magnetic Resonance in Medicine* 13(3): 343–357.

de Graaf, R. (1998). *In vivo NMR Spectroscopy – Principles and Techniques*, Wiley: Chichester.

De Neuter, B., Luts, J., L., V., Lemmerling, P. & Van Huffel, S. (2007). Java-based framework for processing and displaying short-echo-time Magnetic Resonance Spectroscopy signals, *Computer Methods and Programs in Biomedicine* 85: 129–137.

Devos, A., Lukas, L., Suykens, J., Vanhamme, L., Tate, A., Howe, F., Majós, C., Moreno-Torres, A., van der Graaf, M., Arús, C. & Huffel, S. V. (2004). Classification of brain tumours using short echo time ^{1}H MR spectra, *Journal of Magnetic Resonance* 170(1): 164 – 175.

Dologlou, I., Van Huffel, S. & Van Ormondt, D. (1998). Frequency-selective MRS data quantification with frequency *Prior Knowledge*, *Journal of Magnetic Resonance* 130(2): 238 – 243.

Dong, Z., Dreher, W. & Leibfritz, D. (2006). Toward quantitative short-echo-time *in vivo* proton MR spectroscopy without water suppression, *Magnetic Resonance in Medicine* 55(6): 1441–1446.

Eilers, P. H. C. & Marx, B. D. (1996). Flexible smoothing with B-splines and penalties, *Statistical Science* 11: 89–121.

Elster, C., Schubert, F., Link, A., Walzel, M., Seifert, F. & Rinneberg, H. (2005). Quantitative Magnetic Resonance Spectroscopy: Semi-parametric modeling and determination of uncertainties, *Magnetic Resonance in Medicine* 53(6): 1288–1296.

Gabr, R. E., Ouwerkerk, R. & Bottomley, P. A. (2006). Quantifying *in vivo* MR spectra with circles, *Journal of Magnetic Resonance* 179(1): 152 – 163.

Giskeødegård, G. F., Bloemberg, T. G., Postma, G., Sitter, B., Tessem, M.-B., Gribbestad, I. S., Bathen, T. F. & Buydens, L. M. (2010). Alignment of high resolution magic angle spinning magnetic resonance spectra using warping methods, *Analytica Chimica Acta* 683(1): 1 – 11.

Gruetter, R. (1993). Automatic localized *in vivo* adjustment of all first- and second- order shim coils, *Magnetic Resonance in Medicine* 29(6): 804–811.

Guo, Y., Ruan, S., Landré, J. & Constans, J. M. (2010). A sparse representation method for Magnetic Resonance Spectroscopy quantification, *IEEE Transactions on Biomedical Engineering* 57(7): 1620 –1627.

Hao, J., Zou, X., Wilson, M. P., Davies, N. P., Sun, Y., Peet, A. C. & Arvanitis, T. N. (2009). A comparative study of feature extraction and blind source separation of

independent component analysis (ICA) on childhood brain tumour ^{1}H magnetic resonance spectra, *NMR in Biomedicine* 22(8): 809–818.

Hiltunen, Y., Kaartinen, J., Pulkkinen, J., Häkkinen, A.-M., Lundbom, N. & Kauppinen, R. A. (2002). Quantification of human brain metabolites from *in vivo* ^{1}H NMR magnitude spectra using automated artificial neural network analysis, *Journal of Magnetic Resonance* 154(1): 1 – 5.

Hofmann, L., Slotboom, J., Boesch, C. & Kreis, R. (2001). Characterization of the macromolecule baseline in localized ^{1}H-MR spectra of human brain, *Magnetic Resonance in Medicine* 46(5): 855–863.

Hu, S.-L. J., Bao, X. & Li, H. (2010). Model order determination and noise removal for modal parameter estimation, *Mechanical Systems and Signal Processing* 24(6): 1605 – 1620.

Huang, W., Alexander, G. E., Chang, L., Shetty, H. U., Krasuski, J. S., Rapoport, S. I. & Schapiro, M. B. (2001). Brain metabolite concentration and dementia severity in Alzheimer's disease, *Neurology* 57(4): 626–632.

Jiru, F. (2008). Introduction to post-processing techniques, *European journal of radiology* 67(2): 202–217.

Juchem, C., Nixon, T. W., McIntyre, S., Rothman, D. L. & de Graaf, R. A. (2010). Magnetic field homogenization of the human prefrontal cortex with a set of localized electrical coils, *Magnetic Resonance in Medicine* 63(1): 171–180.

Kelm, B. (2007). *Evaluation of Vector-Valued Clinical Image Data Using Probabilistic Graphical Models: Quantification and Pattern Recognition*, PhD thesis.

Klose, U. (1990). *In vivo* proton spectroscopy in presence of eddy currents, *Magnetic Resonance in Medicine* 14(1): 26 – 30.

Knight-Scott, J. (1999). Application of multiple inversion recovery for suppression of macromolecule resonances in short echo time ^{1}H NMR spectroscopy of human brain, *Journal of Magnetic Resonance* 140(1): 228 – 234.

Kunz, N., Cudalbu, C., Mlynárik, V., Hüppi, P. S., Sizonenko, S. V. & Gruetter, R. (2010). Diffusion-weighted spectroscopy: A novel approach to determine macromolecule resonances in short-echo time ^{1}H-MRS, *Magnetic Resonance in Medicine* 64(4): 939–946.

Laudadio, T., Mastronardi, N., Vanhamme, L., Hecke, P. V. & Huffel, S. V. (2002). Improved Lanczos algorithms for blackbox MRS data quantitation, *Journal of Magnetic Resonance* 157(2): 292 – 297.

Laudadio, T., Selén, Y., Vanhamme, L., Stoica, P., Hecke, P. V. & Huffel, S. V. (2004). Subspace-based MRS data quantitation of multiplets using *prior knowledge*, *Journal of Magnetic Resonance* 168(1): 53 – 65.

Lazariev, A., Allouche, A.-R., Aubert-Frécon, M., Fauvelle, F., Elbayed, K., Piotto, M., Namer, I. J., van Ormondt, D. & Graveron-Demilly, D. (2011). Optimization of metabolite basis-sets prior to quantitation: a quantum mechanics approach, *Proc. of the 19th International Society of Magnetic Resonance in Medicine - ISMRM 2011*.

Lin, Y.-Y., Hodgkinson, P., Ernst, M. & Pines, A. (1997). A novel detection-estimation scheme for noisy NMR signals: Applications to delayed acquisition data, *Journal of Magnetic Resonance* 128(1): 30 – 41.

Maudsley, A. A. (1995). Spectral lineshape determination by self-deconvolution, *Journal of Magnetic Resonance, series B* 106(1): 47 – 57.

Metz, K. R., Lam, M. M. & Webb, A. G. (2000). Reference deconvolution: A simple and effective method for resolution enhancement in Nuclear Magnetic Resonance Spectroscopy, *Concepts in Magnetic Resonance* 12(1): 21–42.

Metzger, G. J., Patel, M. & Hu, X. (1996). Application of genetic algorithms to spectral quantification, *Journal of Magnetic Resonance, Series B* 110(3): 316 – 320.

Mierisová, S. & Ala-Korpela, M. (2001). MR Spectroscopy quantitation: a review of frequency domain methods, *NMR in Biomedicine* 14(4): 247–259.

Mlynárik, V., Cudalbu, C., Xin, L. & Gruetter, R. (2008). ^{1}H NMR Spectroscopy of rat brain *in vivo* at 14.1 Tesla: Improvements in quantification of the neurochemical profile, *Journal of Magnetic Resonance* 194(2): 163 – 168.

Osorio-Garcia, M. (2011). *Advanced signal processing for Magnetic Resonance Spectroscopy*, PhD thesis.

Osorio-Garcia, M. I., Sima, D. M., Nielsen, F. U., Himmelreich, U. & Van Huffel, S. (2011). Quantification of Magnetic Resonance Spectroscopy signals with lineshape estimation, *Journal of Chemometrics* 25(4): 183–192.

Papy, J.-M., De Lathauwer, L. & Van Huffel, S. (2007). A shift invariance-based order-selection technique for exponential data modelling, *IEEE Signal Processing Letters* 14(7).

Pels, P. (2005). *Analysis and Improvement of Quantification Algorithms for Magnetic Resonance Spectroscopy*, PhD thesis.

Pfeuffer, J., Tkáč, I., Provencher, S. & Gruetter, R. (1999). Toward an *in vivo* neurochemical profile: Quantification of 18 metabolites in short-echo-time ^{1}H NMR spectra of the rat brain, *Journal of Magnetic Resonance* 141(1): 104 – 120.

Pijnappel, W. W. F., van den Boogaart, A., de Beer, R. & van Ormondt, D. (1992). SVD-based quantification of Magnetic Resonance signals, *Journal of Magnetic Resonance (1969)* 97(1): 122 – 134.

Popa, E., Karras, D., Mertzios, B., Sima, D., de Beer, R., van Ormondt, D. & Graveron-Demilly, D. (2011). Semi-parametric estimation without searching in function space. Application to *in vivo* metabolite quantitation, *Measurement Science and Technology* (Epub) ahead of print, 2011.

Poullet, J.-B. (2008). Spid: Simulation Package based on *in vitro* databases.
URL: *http://homes.esat.kuleuven.be/ biomed/software.php*

Poullet, J.-B., Sima, D. M., Simonetti, A. W., De Neuter, B., Vanhamme, L., Lemmerling, P. & Van Huffel, S. (2007). An automated quantitation of short echo time MRS spectra in an open source software environment: AQSES, *NMR in Biomedicine* 20(5): 493–504.

Poullet, J.-B., Sima, D. M. & Van Huffel, S. (2008). MRS signal quantitation: A review of time- and frequency-domain methods, *Journal of Magnetic Resonance* 195(2): 134 – 144.

Provencher, S. W. (1993). Estimation of metabolite concentrations from localized *in vivo* proton NMR spectra, *Magnetic Resonance in Medicine* 30(6): 672–679.

Provencher, S. W. (2001). Automatic quantitation of localized *in vivo* ^{1}H spectra with LCModel, *NMR Biomed.* 14(4): 260–264.

Ratiney, H., Coenradie, Y., Cavassila, S., van Ormondt, D. & Graveron-Demilly, D. (2004). Time-domain quantitation of ^{1}H short echo-time signals: background accommodation, *Magnetic Resonance Materials in Physics, Biology and Medicine* 16: 284–296.

Ratiney, H., Sdika, M., Coenradie, Y., Cavassila, S., Ormondt, D. v. & Graveron-Demilly, D. (2005). Time-domain semi-parametric estimation based on a metabolite basis set, *NMR in Biomedicine* 18(1): 1–13.

Reynolds, G., Wilson, M., Peet, A. & Arvanitis, T. N. (2006). An algorithm for the automated quantitation of metabolites in *in vitro* NMR signals, *Magnetic Resonance in Medicine* 56(6): 1211–1219.

Romano, R., Motta, A., Camassa, S., Pagano, C., Santini, M. T. & Indovina, P. L. (2002). A new time-domain frequency-selective quantification algorithm, *Journal of Magnetic Resonance* 155(2): 226 – 235.

Ruiz-Pena, J. L., Pinero, P., Sellers, G., Argente, J., Casado, A., Foronda, J., Ucles, A. & Izquierdo, G. (2004). Magnetic resonance spectroscopy of normal appearing white matter in early relapsing-remitting multiple sclerosis: correlations between disability and spectroscopy, *BMC Neurology* 4(1): 8.

Seeger, U., Klose, U., Mader, I., Grodd, W. & Nägele, T. (2003). Parameterized evaluation of macromolecules and lipids in proton MR Spectroscopy of brain diseases, *Magnetic Resonance in Medicine* 49(1): 19–28.

Sima, D. M., Osorio-Garcia, M. I., Poullet, J.-B., Suvichakorn, A., Antoine, J.-P., Huffel, S. V. & van Ormondt, D. (2009). Lineshape estimation for Magnetic Resonance Spectroscopy (MRS) signals: self-deconvolution revisited, *Measurement Science and Technology* 20(10): 104031.

Sima, D. M. & Van Huffel, S. (2007). Separable nonlinear least squares fitting with linear bound constraints and its application in magnetic resonance spectroscopy data quantification, *Journal of Computational and Applied Mathematics* 203: 264–278.

Slotboom, J., Boesch, C. & Kreis, R. (1998). Versatile frequency domain fitting using time domain models and *prior knowledge*, *Magnetic Resonance in Medicine* 39(6): 899–911.

Soher, B. J., Young, K., Govindaraju, V. & Maudsley, A. A. (1998). Automated spectral analysis III: Application to *in vivo* proton MR spectroscopy and spectroscopic imaging, *Magnetic Resonance in Medicine* 40(6): 822–831.

Stefan, D., Di Cesare, F., Andrasescu, A., Popa, E., Lazariev, A., Vescovo, E., Strbak, O., Williams, S., Starčuk, Z., Cabanas, M., van Ormondt, D. & Graveron-Demilly, D. (2009). Quantitation of Magnetic Resonance Spectroscopy signals: the jMRUI software package, *Measurement Science and Technology* 20(10): 104035.

Stoyanova, R. & Brown, T. R. (2001). NMR spectral quantitation by Principal Component Analysis, *NMR in Biomedicine* 14(4): 271–277.

Sundin, T., Vanhamme, L., Van Hecke, P., Dologlou, I. & Van Huffel, S. (1999). Accurate quantification of ^{1}H spectra: From finite impulse response filter design for solvent suppression to parameter estimation, *Journal of Magnetic Resonance* 139(2): 189 – 204.

van den Boogaart, A. (1997). Quantitative data analysis of *in vivo* MRS data sets, *Magnetic Resonance in Chemistry* 35(13): 146–152.

van der Veen, J. W., de Beer, R., Luyten, P. R. & van Ormondt, D. (1988). Accurate quantification of *in vivo* ^{31}P NMR signals using the variable projection method and *prior knowledge*, *Magnetic Resonance in Medicine* 6(1): 92–98.

Van Huffel, S. & Vandewalle, J. (1991). *The Total Least Squares Problem: Computational Aspects and Analysis*, SIAM.

Vanhamme, L., Huffel, S. V., Hecke, P. V. & van Ormondt, D. (1999). Time-domain quantification of series of biomedical magnetic resonance spectroscopy signals, *Journal of Magnetic Resonance* 140(1): 120 – 130.

Vanhamme, L., Sundin, T., Van Hecke, P. & Van Huffel, S. (2001). MR spectroscopy quantitation: a review of time-domain methods, *NMR in Biomedicine* 14(4): 233–246.

Vanhamme, L., van den Boogaart, A. & Van Huffel, S. (1997). Improved method for accurate and efficient quantification of MRS data with use of *Prior Knowledge*, *Journal of Magnetic Resonance* 129(1): 35 – 43.

Vermathen, P., Laxer, K. D., Schuff, N., Matson, G. B. & Weiner, M. W. (2003). Evidence of neuronal injury outside the medial temporal lobe in temporal lobe epilepsy: N-Acetylaspartate concentration reductions detected with multisection Proton MR Spectroscopic Imaging - Initial experience, *Radiology* 226(1): 195–202.

Veselkov, K. A., Lindon, J. C., Ebbels, T. M. D., Crockford, D., Volynkin, V. V., Holmes, E., Davies, D. B. & Nicholson, J. K. (2009). Recursive segment-wise peak alignment of biological ^{1}H NMR spectra for improved metabolic biomarker recovery, *Analytical Chemistry* 81(1): 56–66.

Wilson, M., Reynolds, G., Kauppinen, R. A., Arvanitis, T. N. & Peet, A. C. (2011). A constrained least-squares approach to the automated quantitation of *in vivo* ^{1}H Magnetic Resonance Spectroscopy data, *Magnetic Resonance in Medicine* 65(1): 1–12.

Xi, Y. & Rocke, D. (2008). Baseline correction for NMR spectroscopic metabolomics data analysis, *BMC Bioinformatics* 9(1): 324.

Young, K., Govindaraju, V., Soher, B. J. & Maudsley, A. A. (1998). Automated spectral analysis I: Formation of *a priori* information by spectral simulation, *Magnetic Resonance in Medicine* 40(6): 812–815.

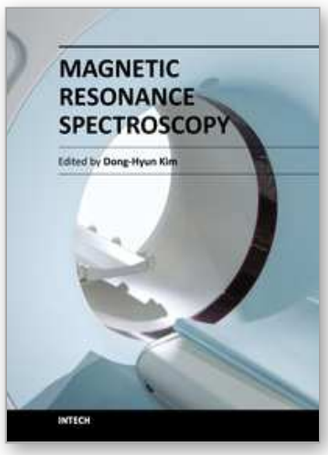

Magnetic Resonance Spectroscopy

Edited by Prof. Dong-Hyun Kim

ISBN 978-953-51-0065-2
Hard cover, 264 pages
Publisher InTech
Published online 02, March, 2012
Published in print edition March, 2012

Magnetic Resonance Spectroscopy (MRS) is a unique tool to probe the biochemistry in vivo providing metabolic information non-invasively. Applications using MRS has been found over a broad spectrum in investigating the underlying structures of compounds as well as in determining disease states. In this book, topics of MRS both relevant to the clinic and also those that are beyond the clinical arena are covered. The book consists of two sections. The first section is entitled 'MRS inside the clinic' and is focused on clinical applications of MRS while the second section is entitled 'MRS beyond the clinic' and discusses applications of MRS in other academic fields. Our hope is that through this book, readers can understand the broad applications that NMR and MRS can offer and also that there are enough references to guide the readers for further study in this important topic.

InTech Europe
University Campus STeP Ri
Slavka Krautzeka 83/A
51000 Rijeka, Croatia
Phone: +385 (51) 770 447
Fax: +385 (51) 686 166
www.intechopen.com

InTech China
Unit 405, Office Block, Hotel Equatorial Shanghai
No.65, Yan An Road (West), Shanghai, 200040, China
中国上海市延安西路65号上海国际贵都大饭店办公楼405单元
Phone: +86-21-62489820
Fax: +86-21-62489821

IntechOpen